SUPPORTING INFORMATION TEXT

SUPPORTING MATERIALS & METHODS

Molecular biology

To optically track the movement of each VSD in $\alpha_{1C\text{-}77}$, a single Cys was substituted at positions at the extracellular flanks of S4 helices in VSDs I (F231C), II (L614C), III (V994C) or IV (S1324C) (Fig.1D) for subsequent modification by thiol-reactive fluorescent labels. Single-point mutations were generated with QuikChange Site-Directed Mutagenesis Kit (Stratagene) and confirmed by sequencing. cRNA was transcribed *in vitro* (mMESSAGE MACHINE; Ambion) and stored at –80 °C.

Oocyte preparation & labeling

Xenopus laevis (Nasco) oocytes (stage V-VI) were prepared as previously described (1) and injected with 50 nl of total cRNA (0.1-0.4μg/μl) using a Drummond nanoinjector. Injected oocytes were maintained at 18 °C in an amphibian saline solution supplemented with 50 μg/ml gentamycin (Gibco). 3-4 days after injection, oocytes expressing channels with Cys substitutions in VSDs I, III or IV were stained for 2 minutes with 20 μM membrane-impermeable, thiol-reactive fluorophore MTS-TAMRA (Santa Cruz Biotechnology) in a depolarizing solution (in mM: 120 K-Methanesulfonate (MES), 2 $Ca(MES)_2$, and 10 HEPES, pH=7.0). Fluorophore tetramethylrhodamine-5′-maleimide (TMRM; Invitrogen) was used to label the VSD II S4 as it produced higher F than MTS-TAMRA, by incubating oocytes with 10 μM label for 20 minutes. Both labels have the same rhodamine fluorescent core but differ in their Cys conjugation moiety. Fluorophore stocks were dissolved in DMSO (100 mM) and stored at –20°C. Following fluorescent labeling, the oocytes were rinsed in dye-free solution.

Electrophysiological Techniques

We used Cut-open Oocyte Vaseline Gap (COVG) voltage clamp complemented with epifluorescence apparatus to simultaneously acquire ionic or gating currents and fluorescence emission, as previously described (2-7). To prevent activation of endogenous Ca^{2+}/Ba^{2+}-activated Cl^{-} channels.Ca^{2+}-dependent inactivation, oocytes were injected with 100 nl 10 nmol BAPTA•4K and 1 nmol HEPES (pH=7.0; final [BAPTA] ≈ 10 mM). External solution (mM): 110 Na-MES, 2 $Ba(MES)_2$, 10 Na-HEPES and 0.1 ouabain (pH=7.0). Internal solution (mM): 110 K-Glutamate, 10 HEPES (pH=7.0). Intracellular micropipette solution (mM): 2700 Na-MES, 10 NaCl and 10 Na-HEPES (pH=7.0). Low access resistance to the oocyte interior was obtained by permeabilizing the oocyte with 0.1% saponin carried by the internal solution. Gating currents were acquired by substituting 2mM $Ba(MES)_2$ in the external solution (recording and guard shield chambers) with 2mM $Co(MES)_2$. The difference in charge screening between 2 Ba^{2+} and 2 Co^{2+} solutions was corrected by comparing F reported from VSD III.

Voltage Dependence & Kinetics Analysis

Experimental data were recorded and analyzed using a customized program developed in our Department. The voltage dependence of channel opening (normalized G(V)) was obtained from the peak tail current at –40 mV and plotted against the test potential. Data for the membrane conductance (G), gating charge displacement (Q), and fluorescence deflection (F) quasi-steady-state curves were fitted to the Boltzmann function given by $A(V) = K/(1+K)$, where $K = \exp(z(V_m - V_{0.5})/kT)$, z is the valence, $V_{0.5}$ is the half-activation potential, V_m is the membrane potential, and kT has its usual thermodynamic significance. and normalized as previously (2, 4-6, 8, 9). In the case of the G(V) curve, the sum of two Boltzmann functions was required for a satisfactory fit.

Current or fluorescence records were fit to a single, or the sum of two exponential functions. Only F with sufficient signal-to-noise ratio (S:N > 2) were included in the kinetics statistics. S:N is defined as mean signal amplitude divided by the root mean square. Fitting was performed by least squares using Microsoft Excel.

Models of Ca_V activation

All models consist of four non-identical voltage sensors J_1...J_4 coupled to a central pore L that is weakly voltage-dependent.

We initially consider the limit of very strong coupling, in which pore opening is contingent upon a specific subset of voltage sensors being activated. Specifically, we tested conditions where the following VSDs were required to activate before channel opening: All four (Fig.4, Scheme I); VSDs I, II and III (Scheme II); and VSDs II and III (Scheme III).

We also considered an allosteric-type model where the pore may open independently, so all open states are accessible, giving rise to the 'cat's cradle' model (Fig.4, Scheme IV). Coupling factors D_1...D_4 (10) are related to interaction energies between W_i through:

$$D_i = \exp(-W_i/kT) \qquad [1]$$

Thermodynamics

The equilibrium constant of pore activation is given by $L = \exp(\gamma_L/kT)$, where $\gamma_L = \Delta q_L(V-V_L)$ is the energetic "bias" of intrinsic pore opening. Similar expressions apply to the voltage sensors $J_i = \exp(\gamma_i/kT)$.

The partition function governing channel gating (11) is given by $Z = Z_c + LZ_o$, where:

$$Z_c = (1+J_1)(1+J_2)(1+J_3)(1+J_4). \qquad [2]$$

The definition of Z_o varies with the type of coupling. For the obligatory gating model with four VSDs (Fig.4, Scheme I), Z_o is defined as:

$$Z_o = J_1\, J_2\, J_3\, J_4. \qquad [3]$$

For the gating model with VSDs I, II and III obligatorily coupled to opening (Fig.4, Scheme II):

$$Z_o = J_1\, J_2\, J_3(1+J_4). \quad [4]$$

For the gating model with VSDs II and III obligatorily coupled to opening (Fig.4, Scheme III):

$$Z_o = (1+J_1)\, J_2\, J_3(1+J_4). \quad [5]$$

And for the allosteric model (Fig.4, Scheme IV):

$$Z_o = (1+J_1D_1)\,(1+J_2D_2)\,(1+J_3D_3)\,(1+J_4D_4). \quad [6]$$

Activity curves for the six particle transitions are obtained from Z through differentiation. For example, $\phi_L \equiv \partial \ln Z/\partial \ln L = LZ_o/Z$, with analogous derivations for the equilibrium constants J_1, J_2, J_3 and J_4. All ϕ have range (0..1). The equilibrium G(V) and Q(V) curves are linear functions of the particle activities:

$$G = G_{min} + (G_{max} - G_{min})\phi_L \quad [7]$$

$$Q = Q_{min} + N(\Delta q_L\phi_L + \Delta q_1\phi_1 + \Delta q_2\phi_2 + \Delta q_3\phi_3 + \Delta q_4\phi_4) \quad [8]$$

where G_{min} and Q_{min} are baseline conductances and gating charges (to be subtracted off as part of experimental analysis) and $G_{max} - G_{min} = Ng$, where N is the number of channels and g is the single channel conductance (assumed voltage-independent).

The fluorescence curves are similarly defined:

$$F_i = F_{i\,min} + \Delta F_i\phi_i \quad [9]$$

The equilibrium curves are generally normalized to the range {0..1}. We define the open probability curve P_o(V) as the unit-normalized G(V) curve, which is also the activity curve for L:

$$P_o = \phi_L = (G - G_{min})/(G_{max} - G_{min}) \quad [10]$$

Kinetics

Expanding the Ca_V model to a kinetic scheme requires specifying rates of activation for each particle. In the case of the pore the forward and backward rate constants are:

$$\alpha_L = \nu_L (LD)^x \quad [11]$$

$$\beta_L = \nu_L (LD)^{x-1} \quad [12]$$

where ν_L is a frequency and x is the proportion of the perturbation energy applied to the forward rate, related to the position of the pore transition barrier (11-14). For an allosteric model, the coupling parameter is $D = D_1^{n_1} D_2^{n_2} D_3^{n_3} D_4^{n_4}$, where n_i is 0 if the i^{th} voltage sensor is at rest, and 1 if it is activated. In obligatory models (Fig.4, Schemes I, II or III) coupling is implicit in the specific form of the kinetic scheme, and $D = 1$. We note that the ratio α_L/β_L yields the expected equilibrium ratio. Similar expression are used for voltage sensor transitions, where $D = D_i$ for the i^{th} voltage sensor in the allosteric model.

The time courses of gating and ionic currents and the fluorescence traces were obtained by numerically integrating the master equation $d\mathbf{p}/dt = \mathbf{pQ}$, where **p** is the row vector of state probabilities p_j and **Q** is the "Q" matrix (15). There are 17 kinetic states for Scheme I; 18 for Scheme II; 20 for Scheme III and 32 ($=2^5$) for Scheme IV (Fig.4).

The linear background-subtracted ionic (I) and gating (I_g) currents were computed according to:

$$I = N \sum_j p_j g_j (V - V_{rev}) \quad [13]$$

$$I_g = N \sum_j \frac{dp_j}{dt} q_j \quad [14]$$

where g_j and q_j are the state conductances and gating charge displacements, respectively. Unitary conductance was set to 0.5 pS. Membrane current (I_m) output was calculated as:

$$I_m = I_g + I_{Coeff} \cdot I \qquad [15]$$

Where I_{Coeff} is a free scaling factor to compensate for null channels, and the real maximal P_{O} and single-channel conductance, and varied between 0.21 (Scheme III) and 0.28 (Scheme I). The "number of channels" was ~1.5E8. While plausible since recording from *Xenopus* oocytes, this quantity is unreliable due to the unknown maximal P_{O} and single-channel conductance.

The unit-normalized fluorescence curves were obtained from:

$$F_i = \sum_j p_j f_{ij} \qquad [16]$$

where the f_i are 0 in resting fluorescent states, and 1 in activated fluorescent states.

The time constant of the simulated voltage pulse was set to 45 μs, which was the measured time constant of voltage steps in the cut-open oocyte clamp filtered at 4 kHz.

Datasets & curve fitting

Fluorescence traces were background-subtracted prior normalization for model fitting. The normalization was performed as follows:

$$F_{norm} = F(-90) + \left(\frac{F}{F_{\max}} - F(-90) \right) \times F(TP) \qquad [17]$$

Where F is the background-subtracted fluorescence data; $F_{\max}$ is the fluorescence recorded at the end of the test pulse (maximum ΔF); $F(-90)$ and $F(\mathrm{TP})$ were obtained from the normalized F(V) data (Fig.3A): they were the mean, normalized steady-state fluorescence values at –90 mV and the test potential, respectively.

The following datasets (45 steady-state and 25 kinetic datasets in total) were fit simultaneously using the Berkeley Madonna curve-fitting function with the models formulated above:

- Mean, normalized, steady-state values at –120, –90, –40, –70, –20, 0, 20, 40, 60 mV for macroscopic conductance and normalized fluorescence from each VSD, to describe the quasi-steady-state F(V) and G(V) curves.
- Representative membrane current and VSD-specific fluorescence traces sampled at 4 kHz and normalized according to the activation level at –90 mV (holding potential) and each test potential (–40, –20, 0, 20 and 40 mV), which included information on both voltage and time dependence.

Berkeley Madonna fit datasets by minimizing the sum of square of the differences between the data and the model predictions. Each dataset was assigned a weight that resulted in satisfactory final fit. *E.g.*, the fluorescence traces, which were relatively noisy, were more tolerant of mis-fitting than the steady-state projections, and Berkeley Madonna could terminate the fitting with an unsatisfactory solution for these traces. In this case, the fitting was repeated with a higher assigned weight. After multiple iterations of initial parameter choices and weight assignments, the best overall fit was chosen.

Hill analysis

The conductance Hill energy $W_{H[g]}$ is a logarithmic transformation of the G(V) curve that provides information about intrinsic pore activation and the coupling between the pore and voltage sensors (11, 16). It is defined as:

$$W_{H[g]} \equiv kT\ln[P_o/(1-P_o)] = kT\ln[(G - G_{min})/(G_{max} - G)] \quad [18]$$

In the case of weak allosterism (Scheme IV), one can resolve the limiting asymptotes of the Hill energy within a reasonable voltage range. These are given by:

$$W_{H[g](-)} \equiv \lim_{V\to-\infty} W_{H[g]} = \gamma_L \quad [19]$$

$$W_{H[g](+)} \equiv \lim_{V\to\infty} W_{H[g]} = \gamma_L - W \quad [20]$$

where $W = W_1 + W_2 + W_3 + W_4$ is total energy of pore-voltage sensor interactions. We note that the slope of both asymptotes is equal to the intrinsic pore charge Δq_L, and the crossing of the negative asymptote on the voltage axis marks the pore's intrinsic half-activation potential V_L. The q_L and V_L values in the allosteric model fitting (Fig.5 & SI Appendix, Fig.S6B) were fixed to the values derived from the Hill transformation of a representative G(V) (SI Appendix, Fig.S6A), constraining the fit.

SUPPORTING REFERENCES

1. Haug T, et al. (2004) Regulation of K^+ flow by a ring of negative charges in the outer pore of BK_{Ca} channels. Part I: Aspartate 292 modulates K^+ conduction by external surface charge effect. *J Gen Physiol* 124(2):173-184.
2. Savalli N, Kondratiev A, Toro L, Olcese R (2006) Voltage-dependent conformational changes in human Ca^{2+}- and voltage-activated K^+ channel, revealed by voltage-clamp fluorometry. *Proc Natl Acad Sci U S A* 103(33):12619-12624.
3. Gandhi CS, Olcese R (2008) The voltage-clamp fluorometry technique. *Methods Mol Biol* 491:213-231.
4. Pantazis A, Gudzenko V, Savalli N, Sigg D, Olcese R (2010) Operation of the voltage sensor of a human voltage- and Ca^{2+}-activated K^+ channel. *Proc Natl Acad Sci U S A* 107(9):4459-4464.
5. Savalli N, Pantazis A, Yusifov T, Sigg D, Olcese R (2012) The contribution of RCK domains to human BK channel allosteric activation. *J Biol Chem* 287(26):21741-21750.
6. Pantazis A, Olcese R (2012) Relative transmembrane segment rearrangements during BK channel activation resolved by structurally assigned fluorophore-quencher pairing. *J Gen Physiol* 140(2):207-218.
7. Pantazis A, Olcese R (2013) Cut-open Oocyte Voltage Clamp Technique. *Encyclopedia of Biophysics*, ed Roberts GCK (Springer, Berlin, Heidelberg), pp 406-413.
8. Savalli N, Kondratiev A, de Quintana SB, Toro L, Olcese R (2007) Modes of operation of the BK_{Ca} channel β2 subunit. *J Gen Physiol* 130(1):117-131.
9. Pantazis A, Kohanteb AP, Olcese R (2010) Relative motion of transmembrane segments S0 and S4 during voltage sensor activation in the human BK(Ca) channel. *J Gen Physiol* 136(6):645-657.
10. Horrigan FT, Aldrich RW (2002) Coupling between voltage sensor activation, Ca^{2+} binding and channel opening in large conductance (BK) potassium channels. *J Gen Physiol* 120(3):267-305.
11. Sigg D (2013) A linkage analysis toolkit for studying allosteric networks in ion channels. *J Gen Physiol* 141(1):29-60.

12. Grosman C, Zhou M, Auerbach A (2000) Mapping the conformational wave of acetylcholine receptor channel gating. *Nature* 403(6771):773-776.

13. Chakrapani S, Auerbach A (2005) A speed limit for conformational change of an allosteric membrane protein. *Proc Natl Acad Sci U S A* 102(1):87-92.

14. Sigg D (2014) Modeling ion channels: past, present, and future. *J Gen Physiol* 144(1):7-26.

15. Colquhoun D, Hawkes AG (1977) Relaxation and fluctuations of membrane currents that flow through drug-operated channels. *Proc R Soc Lond B Biol Sci* 199(1135):231-262.

16. Chowdhury S, Chanda B (2010) Deconstructing thermodynamic parameters of a coupled system from site-specific observables. *Proc Natl Acad Sci U S A* 107(44):18856-18861.

SUPPORTING FIGURE LEGENDS:

Figure S1: $Ca_V1.2$ total charge displacement is composed of the voltage dependences of the four optically-tracked VSDs. Q(V) (▷ and grey curve, as in Fig.3A) and the charge-weighed sum of all F(V) curves (purple curve), *i.e.*: Fweighted= $(F_1(V)*z_1 + F_2(V)*z_2 + F_3(V)*z_3 + F_4(V)*z_4) / (z_1 + z_2 + z_3 + z_4)$; where *z* is the valence of each F(V) from the Boltzmann fit (SI Appendix, Table S1).

Figure S2: Cys mutations and fluorophore labeling minimally perturb $Ca_V1.2$ properties. (A) Membrane currents from wildtype $\alpha_{1C}/\beta_3/\alpha_2\delta$ channels (black) elicited by depolarization to 0 mV are shown superimposed with currents from fluorescently-labeled channels with α_{1C} mutation F231C (to label VSD I, blue), L614C (VSD II, red), V994C (VSD III, green) and S1324C (VSD IV, orange). **(B)** Currents from labeled F231C, L614C, V994C or S1324C labeled channels superimposed with fluorescence traces. To better compare current and fluorescence kinetics, the amplitude of the fluorescence signal was scaled to maximum inward current, as in Fig. 3B. **(C)** As in A, with gating instead of membrane currents. Mean, normalized ionic conductance **(D)** and charge displacement **(E)** plotted against the test potential for wildtype channels (▼), as well as fluorescently-labeled channels with F231C (to label VSD I, ●), L614C (VSD II, ▲), V994C (VSD III, ◆) and S1324C (VSD IV, ■). The curves are single, or the sum of two, Boltzmann distributions for charge displacement and ionic conductance, respectively. Error bars indicate ±S.E.M. Boltzmann parameters are listed in SI Appendix, Table S3.

Figure S3: $Ca_V1.2$ channel opening does not require the activation of four VSDs. (A) Mean, normalized total charge displacement (Q, ▷) ionic conductance (G, ▼) and F reported from VSD I (●), II (▲), III (◆) and IV (■), with super-imposed predictions of Scheme I (curves; model scheme in Fig.4). **(B)** Fluorescence traces recorded from each VSD of $\alpha_{1C}/\beta_3/\alpha_2\delta$ channels for pulses from −90 mV to −40, −20, 0, 20 and 40 mV, normalized to the steady-state probability of activation at every potential. Scheme I predictions are in black.

Note that the timescale for VSD IV traces is 75 ms. **(C)** Membrane current from WT channels (maroon) for the same pulses as in (B), with super-imposed predictions of Scheme I (black). The inset shows the current and model fitting for the –40mV pulse in expanded vertical scale. **(D)** Scheme I fitting parameters.

Figure S4: The activations of VSDs I, II and III is not rate-limiting for $Ca_V1.2$ opening. (A) Mean, normalized total charge displacement (Q, ▷) ionic conductance (G, ▼) and F reported from VSD I (●), II (▲), III (◆) and IV (■), with super-imposed predictions of Scheme II (curves; model scheme in Fig.4). **(B)** Fluorescence traces recorded from each VSD of $\alpha_{1C}/\beta_3/\alpha_2\delta$ channels for pulses from –90 mV to –40, –20, 0, 20 and 40 mV, normalized to the steady-state probability of activation at every potential. Scheme II predictions are in black. Note that the timescale for VSD IV traces is 75 ms. **(C)** Membrane current from WT channels (maroon) for the same pulses as in (B), with super-imposed predictions of Scheme II (black). The inset shows the current and model fitting for the –40mV pulse in expanded vertical scale. **(D)** Scheme II fitting parameters.

Figure S5: The activation of VSDs II and III is obligatory for $Ca_V1.2$ opening. (A) Mean, normalized total charge displacement (Q, ▷) ionic conductance (G, ▼) and F reported from VSD I (●), II (▲), III (◆) and IV (■), with super-imposed predictions of Scheme III (curves; model scheme in Fig.4). **(B)** Fluorescence traces recorded from each VSD of $\alpha_{1C}/\beta_3/\alpha_2\delta$ channels for pulses from –90 mV to –40, –20, 0, 20 and 40 mV, normalized to the steady-state probability of activation at every potential. Scheme III predictions are in black. Note that the timescale for VSD IV traces is 75 ms. **(C)** Membrane current from WT channels (maroon) for the same pulses as in (B), with super-imposed predictions of Scheme III (black). The inset shows the current and model fitting for the –40mV pulse in expanded vertical scale. Scheme III predictions fully account for the voltage- and time-dependent properties of $Ca_V1.2$ VSD activation and pore opening, indicating that the activation of VSDs II and III governs Ca^{2+} conductance. **(D)** Scheme III fitting parameters.

Figure S6: Hill transformation of a representative G(V) & Scheme IV fitting parameters. (A) A characteristic G(V) was Hill-transformed (○) with allosteric model constraints (the positive and negative asymptotes have equal slope), to determine intrinsic pore voltage dependence parameters ($V_{0.5}$=135mV; q=0.76e^0). These values were fixed for the fitting of Scheme IV (Fig.5). **(B)** Scheme IV (Figs.4D & 5) fitting parameters. Parameters q and $V_{0.5}$ for the pore (marked with *) were fixed to values estimated from G(V) Hill analysis.

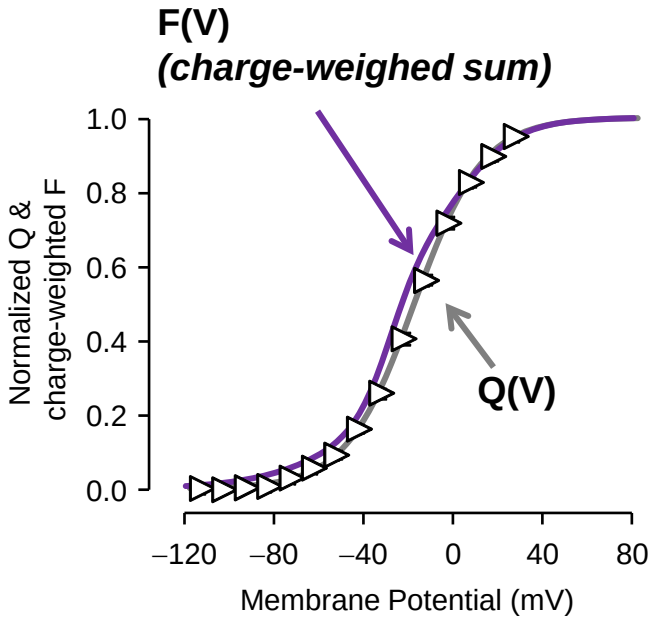
F(V)
(charge-weighed sum)
Normalized Q &
charge-weighted F
1.0
0.8
0.6
0.4
0.2
0.0
Q(V)
−120
−80
−40
0
40
80
Membrane Potential (mV)

Figure S1

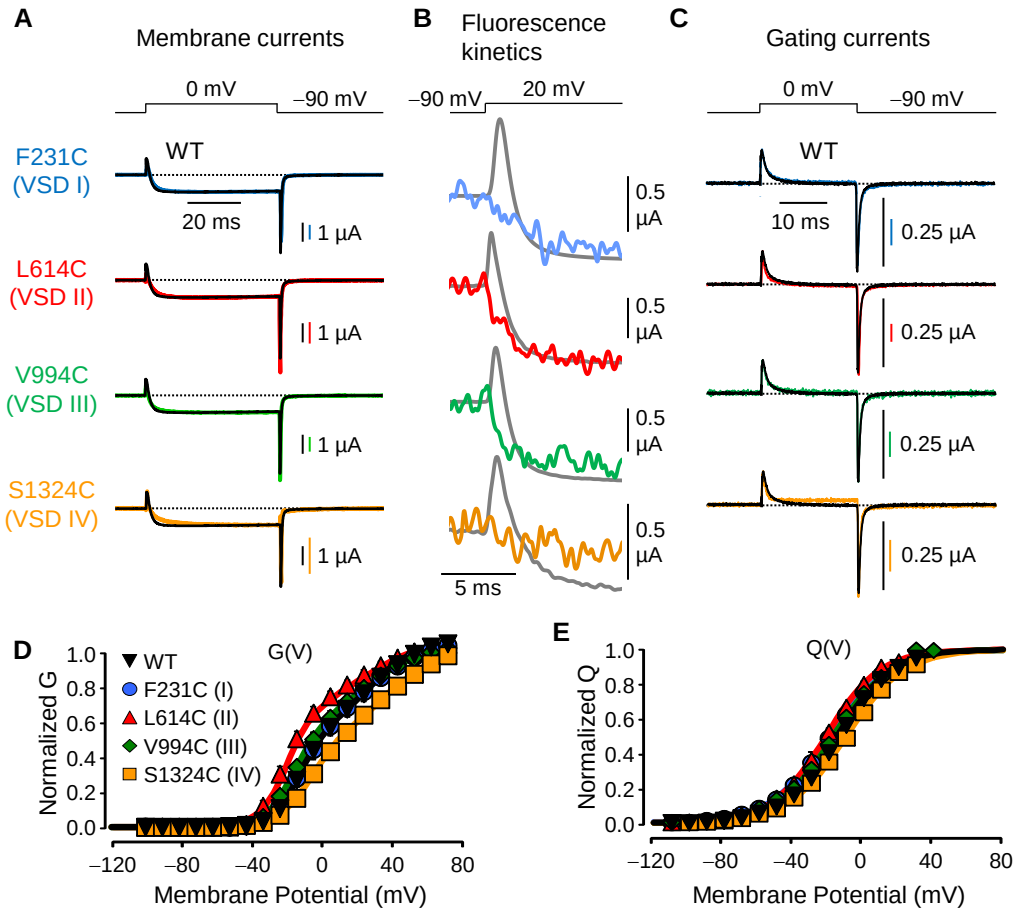
A
Membrane currents
0 mV
–90 mV
WT
F231C
(VSD I)
20 ms
1 µA
L614C
(VSD II)
1 µA
V994C
(VSD III)
1 µA
S1324C
(VSD IV)
1 µA
B
Fluorescence
kinetics
–90 mV
20 mV
0.5
µA
0.5
µA
0.5
µA
0.5
µA
5 ms
C
Gating currents
0 mV
–90 mV
WT
10 ms
0.25 µA
0.25 µA
0.25 µA
0.25 µA
D
G(V)
WT
F231C (I)
L614C (II)
V994C (III)
S1324C (IV)
Normalized G
1.0
0.8
0.6
0.4
0.2
0.0
–120
–80
–40
0
40
80
Membrane Potential (mV)
E
Q(V)
Normalized Q
1.0
0.8
0.6
0.4
0.2
0.0
–120
–80
–40
0
40
80
Membrane Potential (mV)

Figure S2

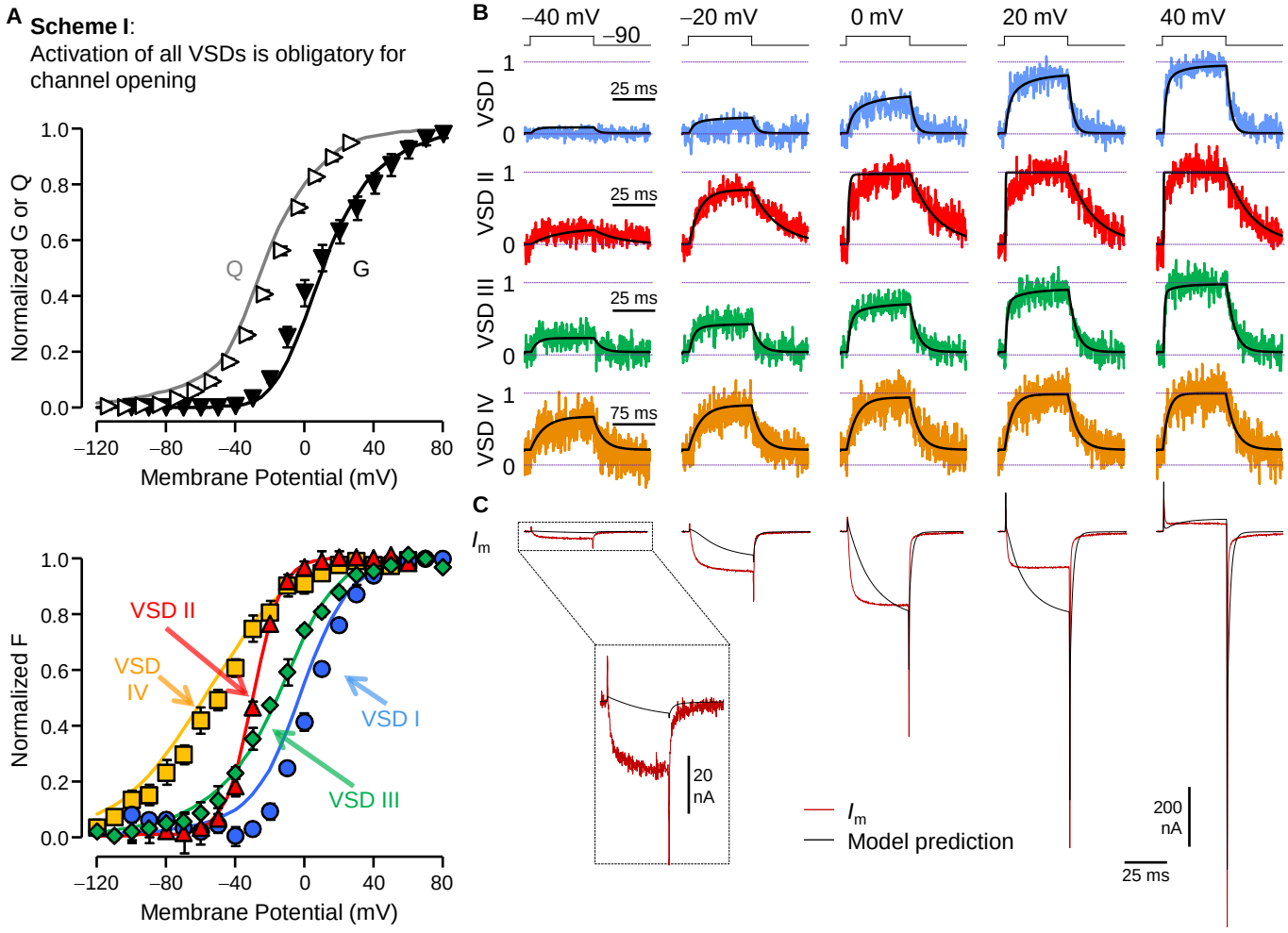

D

	q (e^0)	$V_{0.5}$ (mV)	x	ν (s^{-1})
Pore	0.64	–37	0.0	2100
VSD I	1.1	16	0.85	170
VSD II	3.0	–29	0.95	34
VSD III	1.0	–9.1	1.0	170
VSD IV	1.0	–58	0.40	16

Figure S3

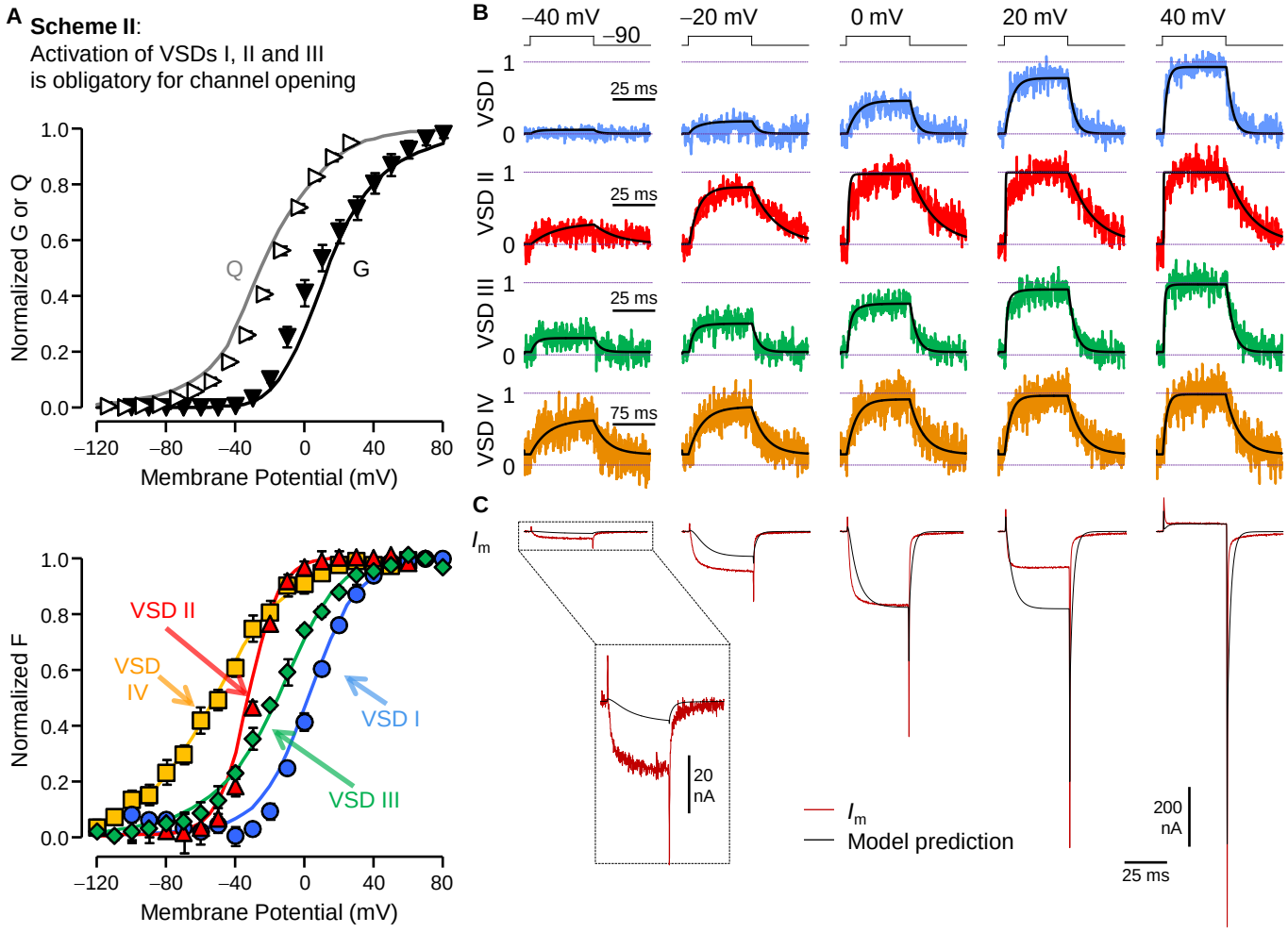

D

	q (e^0)	$V_{0.5}$ (mV)	x	ν (s^{-1})
Pore	0.61	–43	0.04	2900
VSD I	1.1	26	0.96	210
VSD II	2.7	–32	0.93	33
VSD III	1.0	–9.4	1.0	200
VSD IV	1.2	–52	0.54	12

Figure S4

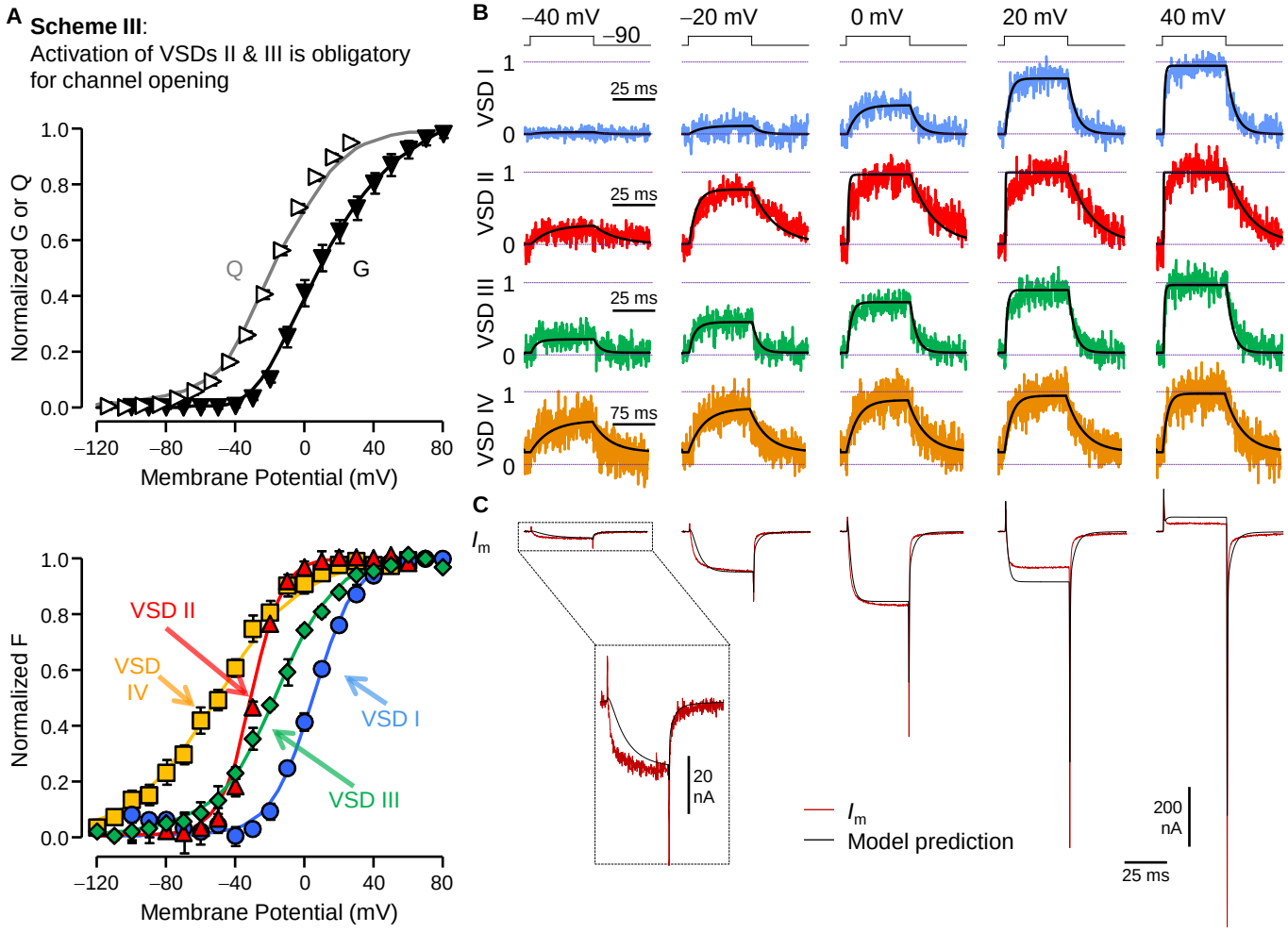

D

	q (e^0)	$V_{0.5}$ (mV)	x	ν (s^{-1})
Pore	0.72	–0.89	0.29	550
VSD I	2.1	5.1	0.91	75
VSD II	2.6	–29	1.0	54
VSD III	1.1	–7.2	1.0	210
VSD IV	1.0	–50	0.60	10

Figure S5

A

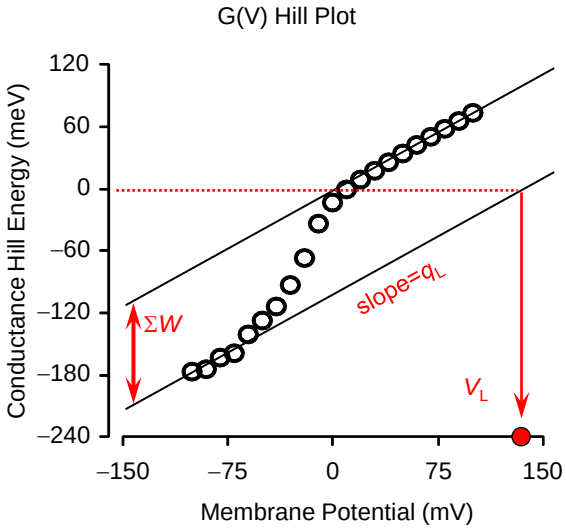

B

Allosteric Model (Scheme IV) Parameters

	q (e^0)	$V_{0.5}$ (mV)	x	ν (s^{-1})	W (meV)
Pore	0.76*	135*	0.49	670	
VSD I	2.0	8.5	0.89	110	–16
VSD II	2.5	–27	0.99	44	–50
VSD III	1.0	–11	0.93	160	–45
VSD IV	1.1	–52	0.55	11	–0.87

Figure S6

SUPPORTING TABLES

VSD	$V_{0.5}$ (mV)	z (e^0)	N
I	5.1±1.3	2.1±0.12	5
II	−28±1.4	3.2±0.42	7
III	−18±2.1	1.4±0.085	7
IV	−52±2.7	1.2±0.093	6

Table S1: Voltage dependence of fluorescence signals from each of the four $Ca_V1.2$ VSDs. F acquired from each VSD was normalized and fit to Boltzmann distributions with parameters listed here. The curves of the distributions are shown in Fig.3A. The Boltzmann distributions of simultaneously-recorded conductance are shown in SI Appendix, Table S3. Errors indicate ±S.E.M.

	ON				OFF				
	τ_1 (ms)	A_1 (%)	τ_2 (ms)	A_2 (%)	τ_1 (ms)	A_1 (%)	τ_2 (ms)	A_2 (%)	N
Current	1.0±0.17	100			0.31±0.034	97±1.3	1.4±0.13	3.3±1.3	3
VSD I	2.2±0.22	65±4.3	14±2.9	35±4.3	3.4±0.87	73±9.5	43±16	27±9.5	3
VSD II	0.99±0.072	64±16	13±3.4	36±16	1.1±0.43	27±8.2	23±3.2	73±8.2	4
VSD III	0.84±0.13	67±5.7	9.0±1.3	33±5.7	5.2±0.61	100			4
VSD IV	21±5.3	100			31±3.6	100			4

Table S2: $Ca_V1.2$ Current and VSD kinetics. The mean time constants (τ) and fractional amplitudes (A) of the exponential timecourse fitting of F reported from VSD I, II, III and IV, upon a depolarization from −90 mV to 20 mV (ON; see Fig.3B) and repolarization to −90 mV (OFF). Ionic currents were isolated before fitting by subtracting the gating current component, acquired in 0.5 mM $Co(MES)_2$ and 0.3 mM $LaCl_3$. Errors indicate ±S.E.M.

	Charge Displacement			Ionic Conductance						
Channel	$V_{0.5}$ (mV)	z (e^0)	N	$V1_{0.5}$ (mV)	$z1$ (e^0)	$A1$ (%)	$V2_{0.5}$ (mV)	$z2$ (e^0)	$A2$ (%)	N
WT	−18±0.47	1.7±0.080	4	−7.0±1.8	3.2±0.35	54±2.7	36±3.2	1.9±0.20	46±2.7	5
F231C	−22±1.0	1.5±0.035	4	−8.5±0.9	3.2±0.10	51±1.3	32±3.7	1.6±0.082	49±1.3	5
L614C	−24±1.6	1.7±0.077	4	−17±1.6	4.1±0.21	58±1.9	25±3.6	1.6±0.059	42±1.9	15
V994C	−20±2.1	1.6±0.19	4	−11±1.7	3.2±0.26	53±3.1	34±5.3	1.7±0.15	47±3.1	7
S1324C	−13±1.6	1.6±0.071	4	−1.0±1.3	2.8±0.23	42±4.2	44±2.7	1.3±0.077	58±4.2	9

Table S3: WT and Cys mutant $Ca_V1.2$ voltage dependence of charge displacement and ionic conductance. The voltage dependence (Boltzmann distribution parameters) of total $Ca_V1.2$ charge displacement (SI Appendix, Fig.S2E) and ionic conductance (SI Appendix, Fig.S2D), for wildtype α_{1C} channels, as well as fluorescently-labeled channels with mutations F231C (to label VSD I), L614C (II), V994C (III) or S1324C (IV). The Boltzmann distributions for simultaneously-recorded F are shown in SI Appendix, Table S1. Errors indicate ±S.E.M.